

Heteroepitaxy of Large-Area, Monocrystalline Lead Halide Perovskite Films on Gallium Arsenide

Deying Kong¹, Yu Zhang², Dali Cheng³, Enze Wang¹, Kaiyuan Zhang³, Huachun Wang³, Kai Liu¹, Lan Yin^{1,*} and Xing Sheng^{3,*}

Affiliations

¹School of Materials Science and Engineering, The Key Laboratory of Advanced Materials of Ministry of Education, State Key Laboratory of New Ceramics and Fine Processing, Center for Flexible Electronics Technology, Tsinghua University, Beijing, China

²Department of Physics, Tsinghua University, Beijing, China

³Department of Electronic Engineering, Beijing National Research Center for Information Science and Technology, Center for Flexible Electronics Technology, IDG/McGovern Institute for Brain Research, Tsinghua University, Beijing, China

*Correspondence to: lanyin@tsinghua.edu.cn; xingsheng@tsinghua.edu.cn

ABSTRACT

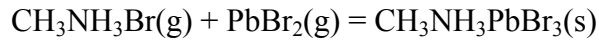
Lead halide perovskite materials have been emerging as promising candidates for high-performance optoelectronic devices. Significant efforts have sought to realize monocrystalline perovskite films at a large scale. Here, we epitaxially grow monocrystalline methylammonium lead tribromide (MAPbBr₃) films on lattice-matched gallium arsenide (GaAs) substrates at a centimeter scale. In particular, a solution-processed lead(II) sulfide (PbS) layer provides a lattice-matched and chemical protective interface for the solid-gas reaction to form MAPbBr₃ films on GaAs. Structure characterizations identify the crystal orientations in the trilayer MAPbBr₃/PbS/GaAs epi-structure and confirm the monocrystalline nature of MAPbBr₃ on PbS/GaAs. The dynamic evolution of surface morphologies during the growth indicates a two-step epitaxial process. These fundamental understandings and practical growth techniques offer a viable guideline to approach high-quality perovskite films for previously inaccessible applications.

MAIN TEXT

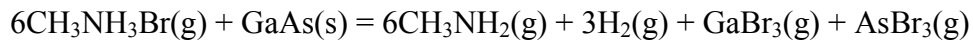
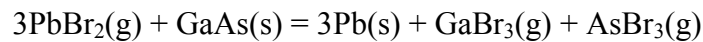
In the past few years, hybrid lead halide perovskites have become promising candidates as new generation semiconductors for advanced optoelectronic materials and devices, including remarkable developments like high-efficiency solar cells and light-emitting diodes (LEDs)^{1, 2, 3, 4, 5}. In spite of these achievements, these devices are mostly based on polycrystalline perovskites, and it is imperative to obtain large-area, single crystalline perovskite films with a high quality on par with traditional semiconductors like silicon (Si) or gallium arsenide (GaAs)^{6, 7, 8, 9}. Certain accomplishments have been achieved, for example, by growing monocrystalline perovskite films via lattice-matched homoepitaxy or metamorphic heteroepitaxy on uncommon substrates like monocrystalline perovskites^{10, 11, 12, 13}, metal halides^{14, 15} or lead chalcogenides^{16, 17}. Other attempts include the growth of perovskite crystals on more common but lattice-mismatched substrates like Si, GaN, quartz, gold, sapphire, etc.^{18, 19, 20, 21, 22, 23}, via spin coating, inkjet printing, mechanical slicing, space-confined crystallization, chemical vapor deposition, electrodeposition, etc.^{20, 22, 23, 24, 25, 26}. However, crystal sizes formed on these lattice-mismatched substrates are limited to scales ranging from several micrometers to several millimeters. In a word, existing approaches either require lattice-matched crystals that are not readily available, or utilize lattice-mismatched substrates that constrain the growth of large-area, monocrystalline perovskite films. In other words, the limited availability of large-area, lattice-matched substrates and their associated growth strategies hinder the formation of large-area, monocrystalline perovskite films, which has long been desired for unprecedented device applications.

In this work, we report the epitaxial growth of centimeter-scale, monocrystalline methylammonium lead tribromide ($\text{CH}_3\text{NH}_3\text{PbBr}_3$, or MAPbBr_3) perovskite films on lattice-matched GaAs wafers. Coincidentally, cubic-phase MAPbBr_3 has a lattice constant ($a = 5.91 \text{ \AA}$)²⁷ close to that of zinc-blende GaAs ($a = 5.65 \text{ \AA}$), making the lattice-matched or

metamorphic epitaxy possible. To evaluate this hypothesis, we first attempt to grow MAPbBr₃ via conventional chemical vapor deposition (CVD)²⁸, following the reaction of methylammonium bromide (CH₃NH₃Br, or MABr) and lead(II) bromide (PbBr₂) at 350 °C (Figure S1a):

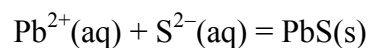


This reaction produces polycrystalline MAPbBr₃ on lattice-mismatched Si (100) substrates ($a = 5.43 \text{ \AA}$) (Figure S1b), which is expected and in accordance with previous reports²⁸. However, the same synthesis process results in the formation of lead (Pb) powders on GaAs (100), which makes the direct CVD growth of MAPbBr₃ unsuccessful (Figure S1c). This observation is likely to be attributed to more favorable reactions between bromides and GaAs at 350 °C^{29,30}:

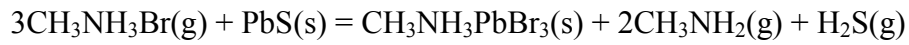


which produce volatile gallium(III) bromide (GaBr₃) and arsenic tribromide (AsBr₃) with boiling points of 278 °C and 221 °C, respectively. In fact, many group III and group V halides form volatile gases (for example, boiling points are 201 °C for GaCl₃, 130 °C for AsCl₃, 173 °C for PBr₃, etc.). Therefore, even if the lattice matching requirement is satisfied, such detrimental processes could prevent the direct epitaxy of various halide perovskites on GaAs at elevated temperatures.

To bypass this challenge, we introduce a lead(II) sulfide (PbS) interface layer to ameliorate the epitaxial growth of MAPbBr₃ on GaAs (Figure 1). The PbS layer is grown on GaAs via chemical bath deposition (CBD) by the reaction of lead and sulfur ions in the alkaline solution (Figure 1a)^{31,32}:



Subsequently, the MAPbBr₃ film is formed by the solid-gas reaction between MABr and PbS in the CVD tube at 145 °C (Figure 1b):



Such a reaction was previously employed for perovskite nanocrystals or quantum dots^{33, 34, 35}, but has not been explored to form large-area monocrystalline perovskite films. The introduction of the PbS interlayer is advantageous in multiple aspects: (1) PbS has a face-centered cubic (FCC), rock salt structure almost perfectly lattice-matched ($a = 5.93 \text{ \AA}$) to MAPbBr₃, working as an ideal buffer layer between MAPbBr₃ ($a = 5.91 \text{ \AA}$) and GaAs ($a = 5.65 \text{ \AA}$); (2) PbS protects GaAs against detrimental reactions with halides; (3) PbS serves as a Pb source and directly reacts with MABr, reducing the CVD temperature from 350 °C to 145 °C. Such material choices and process strategies eventually cause the formation of large-area, monocrystalline MAPbBr₃ on GaAs, which is systematically analyzed subsequently.

Figure 2 presents materials and crystal characterizations for the PbS/GaAs and the MAPbBr₃/PbS/GaAs epitaxial structures. Figures 2a and 2b show that both the PbS and the MAPbBr₃ films form uniform coatings on a GaAs (100) wafer sample with a dimension of around $2 \times 2 \text{ cm}^2$. In addition, the MAPbBr₃ film presents a highly-ordered island structure with cube-shaped crystals all oriented along the cleavage directions ($[110]$ and $[1\bar{1}0]$) of GaAs (100) wafers (Figure 2b, bottom). Cross-sectional scanning electron microscopic (SEM) images (Figure 2c) and corresponding element mappings (Figure S2) indicate that the as-prepared PbS film has a thickness of $\sim 500 \text{ nm}$ after $\sim 5 \text{ min}$ CBD, and the MAPbBr₃ layer is $\sim 200 \text{ nm}$ thick after $\sim 8 \text{ hour}$ CVD. Electron Back Scatter Diffraction (EBSD) mappings (Figure 2d) clearly illustrate that both the PbS and the MAPbBr₃ films have monocrystalline characteristics, with a preferential growth in $[110]$ and $[100]$ directions, respectively. In agreement with EBSD data, out-of-plane x-ray diffraction (XRD) patterns in Figure 2e

confirm that the PbS and the MAPbBr₃ films have growth planes of (220) and (100), respectively. For comparison, the same procedures to grow PbS and MAPbBr₃ films are performed on Si and glass substrates. As expected, XRD results indicate that these films are polycrystalline on Si and glass (Figure S3).

Pole figures in Figure 2f further elucidate in-plane monocrystalline structures for PbS and MAPbBr₃ films. The (111) pole figure of PbS with two spots separated azimuthally by 180° at a tilt angle of 35°, corresponding to the angle between (111) and (220) planes, indicates the in-plane orientation of PbS with respect to GaAs (Figure 2f, top). Additionally, the (211) pole figure of MAPbBr₃ show four spots separated azimuthally by 90° at a tilt angle of 35°, corresponding to the angle between (211) and (100) planes, and eight spots that are divided into two identical rectangular patterns, indicating the fourfold symmetry of the (100) plane. It is noted that the (211) planes are unique for simple-cubic perovskite MAPbBr₃ and do not present in the rock salt structure of PbS or the zinc-blende GaAs. The (211) patterns of MAPbBr₃ rotate by 45° in plane in relation to GaAs [100] direction, indicating the orientation of the MAPbBr₃ crystal. The clearly distinct spot patterns with a low background noise reveal the high quality of monocrystalline PbS and MAPbBr₃ films. Results of reciprocal space mapping (RSM) analysis are obtained around (300) and (331) points of MAPbBr₃ (Figure 2g). The asymmetric feature suggests the existence of different in-plane strains in different directions. Collectively, these experimental results clearly demonstrate the single crystal feature of the MAPbBr₃ film epitaxially formed on the PbS/GaAs substrate.

Monocrystalline GaAs (100) substrates have been extensively used in optoelectronic industry at affordable costs up to 8 inches in diameter³⁶. Its widespread availability promises the potential to scale up the heteroepitaxy of MAPbBr₃ films. Figure 3a presents a MAPbBr₃/PbS/GaAs sample with a size of 1.5 × 5 cm², in which three different locations are independently examined with SEM and XRD. Similar surface morphologies obtained at these

locations indicate that the sample has a very uniform MAPbBr₃ coating (Figure 3b), and consistent XRD peaks of the (211) plane during in-plane phi scanning reveal the single-crystal phase forming across the entire sample surface.

Based on the XRD results obtained in Figure 2, we establish an atomic model to interpret the MAPbBr₃/PbS/GaAs epi-structure, illustrated in Figure 4. The structure data is also provided as a supplemental file. According to Figures 2d–2f, the epitaxial relation is MAPbBr₃ (100) || PbS (110) || GaAs (100), MAPbBr₃ [001] || PbS [001] || GaAs [011], and MAPbBr₃ [010] || PbS [1 $\bar{1}$ 0] || GaAs [01 $\bar{1}$]. Specifically, the PbS layer grows up along its [110] direction on GaAs (100), and in-plane directions [001] and [1 $\bar{1}$ 0] are parallel to GaAs [011] and [01 $\bar{1}$], respectively. This observation is consistent with previous reports³⁷. While there is only a ~5% mismatch between PbS [1 $\bar{1}$ 0] and GaAs [01 $\bar{1}$], the mismatch between PbS [001] and GaAs [011] is as large as ~50%. Therefore, the lattice registry is most likely metamorphic along GaAs [01 $\bar{1}$] and coincident along GaAs [011], forming a superlattice with 3 GaAs and 2 PbS. Similar observations are obtained at the MAPbBr₃/PbS heterointerface. The lattice is almost perfectly matched between MAPbBr₃ [001] and PbS [001], but there is a ~50% mismatch between MAPbBr₃ [010] and PbS [1 $\bar{1}$ 0]. Therefore, the coincident growth along PbS [1 $\bar{1}$ 0] creates a superlattice with 3 PbS and 2 MAPbBr₃. Mechanisms for such a growth preference remain unclear, which are probably ascribed to the different crystal structures of GaAs (zinc blende), PbS (rock salt) and MAPbBr₃ (perovskite).

The epitaxial process for MAPbBr₃ on PbS/GaAs is further investigated by examining the film morphology with SEM and atomic force microscopy (AFM), at different time courses during the growth (Figure 5). The as-grown PbS/GaAs sample has a relatively smooth surface, with a root-mean-square (RMS) roughness of ~5.4 nm (Figure 5a). Observed surface defects are likely related to misfit dislocations. Clearly, the growth of MAPbBr₃ on

PbS/GaAs divides into two distinct steps. In the first step, the solid-gas reaction of MABr and PbS occurs on the PbS surface. After CVD growth for 0.2 hours, a MAPbBr₃ film appears and forms an undulating surface with a period of ~70 nm and a roughness of ~8.5 nm (Figure 5b). In particular, the striped structures follow the cleavage directions of GaAs (100) wafers, which are [110] and [1 $\bar{1}$ 0]. Such an anisotropic growth can be explained by the lattice matching conditions between MAPbBr₃ and PbS, which results in distinct appearance along the two in-plane directions [001] and [010] for MAPbBr₃ (Figure 4). The mechanisms are analogous to the classical Frank–van der Merwe growth in the MAPbBr₃ [001] direction, and the Volmer–Weber growth in the MAPbBr₃ [010] direction³⁸. As the process continues, the MABr gas has to diffuse through the MAPbBr₃ film and reacts with the PbS underneath it. The second step forms more rectangular or cubic shaped MAPbBr₃ crystals and eventually results in a continuous film surface with terrace morphology (Figures 5c and 5d). After CVD growth for 8 hours, the MAPbBr₃ film has a roughness of ~12.6 nm. It is noted that the MAPbBr₃ growth rate considerably decreases as the film becomes thicker, since the film growth is eventually limited by the diffusion of MABr gas into the MAPbBr₃ film. Such growth kinetics is analogous to the thermal oxidation of silicon³⁹.

In summary, we demonstrate the heteroepitaxy of centimeter-scale, monocrystalline MAPbBr₃ films on GaAs (100) via the gas-solid reaction, with a solution-processed PbS interfacial layer. Such a growth strategy overcomes the limitations of previously explored methods, and heterogeneously integrates an emerging lead halide perovskite material with a traditional III–V compound semiconductor, in a single crystal format. The applied CBD and CVD processes, as well as the use of GaAs (100) wafers, are compatible with large-scale manufacturing. It is envisioned that these concepts could immediately realize high-quality monocrystalline perovskites on 6-inch and even 8-inch GaAs wafers. Future possibilities involve the large-area production of many other halide perovskites with similar lattice

structures, for example, MAPbCl₃ ($a = 5.67 \text{ \AA}$), CsPbCl₃ ($a = 5.61 \text{ \AA}$) and CsPbBr₃ ($a = 5.87 \text{ \AA}$). These monocrystalline materials could potentially produce perovskite-based optoelectronic devices with higher performance, although additional issues associated with device design and fabrications must be considered. Collectively, the concepts provide a promising direction for fundamental materials research and advanced device applications.

Methods

PbS growth

PbS films are grown on GaAs (100) wafers (single-side polished, updoped, AXT Inc.) via chemical bath deposition (CBD) at 50 °C in ambient environment (Figure 1a). The chemical solution contains 270 mM sodium hydroxide (NaOH powder, 97%, Alfa Aesar), 10 mM lead nitrate ($\text{Pb}(\text{NO}_3)_2$ powder, 99.99%, Aladdin) and 50 mM thiourea ($\text{SC}(\text{NH}_2)_2$ powder, 99%, Sigma Aldrich). The growth rate is ~ 1 nm/s. The polished side of GaAs faces down in the solution, to avoid PbS cluster particles randomly falling on the growth surface. The PbS deposition is also performed on Si (100) wafers and glass substrates for comparison.

MAPbBr₃ growth on PbS/GaAs

MAPbBr₃ films are formed on PbS/GaAs substrates via chemical vapor deposition (CVD) with a solid-gas reaction (Figure 1b). As-grown PbS/GaAs samples and excessive methylammonium hydrobromide (MABr powder, 98%, TCI Chemicals) are placed in a quartz tube furnace (OTF-1200X-S, tube diameter 50 mm, MTI Corp.) The reaction of MABr and PbS to form MAPbBr₃ occurs at 145 °C in argon environment at a pressure of ~ 100 Pa. The MAPbBr₃ growth is also performed on PbS/Si and PbS/glass substrates for comparison.

MAPbBr₃ growth on Si and GaAs

MAPbBr₃ growth is also attempted on Si and GaAs substrates via traditional CVD methods²⁸ without the PbS interlayer (Figure S1a). Excessive lead bromide (PbBr_2 powder, 99%, TCI Chemicals) and MABr powders are placed in the furnace at 350 °C in the upper stream of Ar flow (30 sccm, 100 Pa), while Si (100) or GaAs (100) wafers are placed in the down stream. The process lasts for ~ 20 mins.

Materials Characterizations

X-ray diffraction (XRD) patterns are obtained with a Rigaku S2 diffractometer (40 kV, 40 mA). Phi scanning are performed using constant 2θ angles corresponding to the MAPbBr₃ (211) diffraction plane. XRD pole figures are measured using constant 2θ angles corresponding to the GaAs/PbS (111) planes and the MAPbBr₃ (211) plane. Asymmetric high-resolution reciprocal space maps (HR RSM) around (300) and (133) points of MAPbBr₃ are plotted with the scanning mode on a Bruker D8 Discover. SEM images are taken with a Zeiss GeminiSEM 500 (15 kV), and EBSD data are measured with a Zeiss Merlin. AFM images are obtained with a BRUKER Multimode 8 (peak-force tapping mode). Atomic structures are established with Materials Studio 8.0 (Accelrys).

REFERENCES

1. Cho H, Jeong S-H, Park M-H, Kim Y-H, Wolf C, Lee C-L, *et al.* Overcoming the electroluminescence efficiency limitations of perovskite light-emitting diodes. *Science* 2015, **350**(6265): 1222-1225.
2. Dou L, Yang Y, You J, Hong Z, Chang W-H, Li G, *et al.* Solution-processed hybrid perovskite photodetectors with high detectivity. *Nature Communications* 2014, **5**(1): 5404.
3. Li X, Bi D, Yi C, Décoppet J-D, Luo J, Zakeeruddin SM, *et al.* A vacuum flash-assisted solution process for high-efficiency large-area perovskite solar cells. *Science* 2016, **353**(6294): 58-62.
4. Chen Q, Wu J, Ou X, Huang B, Almutlaq J, Zhumeckenov AA, *et al.* All-inorganic perovskite nanocrystal scintillators. *Nature* 2018, **561**(7721): 88-93.
5. Akkerman QA, Rainò G, Kovalenko MV, Manna L. Genesis, challenges and opportunities for colloidal lead halide perovskite nanocrystals. *Nature Materials* 2018, **17**(5): 394-405.
6. Saidaminov MI, Abdelhady AL, Murali B, Alarousu E, Burlakov VM, Peng W, *et al.* High-quality bulk hybrid perovskite single crystals within minutes by inverse temperature crystallization. *Nat Commun* 2015, **6**: 7586.

7. Chen J, Morrow DJ, Fu Y, Zheng W, Zhao Y, Dang L, *et al.* Single-Crystal Thin Films of Cesium Lead Bromide Perovskite Epitaxially Grown on Metal Oxide Perovskite (SrTiO₃). *J Am Chem Soc* 2017, **139**(38): 13525-13532.
8. Zou Y, Li F, Zhao C, Xing J, Yu Z, Yu W, *et al.* Anomalous Ambipolar Phototransistors Based on All - Inorganic CsPbBr₃ Perovskite at Room Temperature. *Advanced Optical Materials* 2019, **7**(21).
9. Wang L, King I, Chen P, Bates M, Lunt RR. Epitaxial and quasiepitaxial growth of halide perovskites: New routes to high end optoelectronics. *APL Materials* 2020, **8**(10).
10. Lei Y, Chen Y, Zhang R, Li Y, Yan Q, Lee S, *et al.* A fabrication process for flexible single-crystal perovskite devices. *Nature* 2020, **583**(7818): 790-795.
11. Chen Y, Lei Y, Li Y, Yu Y, Cai J, Chiu MH, *et al.* Strain engineering and epitaxial stabilization of halide perovskites. *Nature* 2020, **577**(7789): 209-215.
12. Lei Y, Chen Y, Gu Y, Wang C, Huang Z, Qian H, *et al.* Controlled Homoepitaxial Growth of Hybrid Perovskites. *Adv Mater* 2018, **30**(20): e1705992.
13. Zhang L, Liu L, Zhang P, Li R, Zhang G, Tao X. Thickness-Controlled Wafer-Scale Single-Crystalline MAPbBr₃ Films Epitaxially Grown on CsPbBr₃ Substrates by the Droplet-Evaporated Crystallization Method. *ACS Appl Mater Interfaces* 2020, **12**(35): 39834-39840.

14. Ji L, Hsu HY, Lee JC, Bard AJ, Yu ET. High-Performance Photodetectors Based on Solution-Processed Epitaxial Grown Hybrid Halide Perovskites. *Nano Lett* 2018, **18(2)**: 994-1000.
15. Jiang J, Sun X, Chen X, Wang B, Chen Z, Hu Y, *et al.* Carrier lifetime enhancement in halide perovskite via remote epitaxy. *Nat Commun* 2019, **10(1)**: 4145.
16. Sytnyk M, Yousefi - Amin AA, Freund T, Prihoda A, Götz K, Unruh T, *et al.* Epitaxial Metal Halide Perovskites by Inkjet - Printing on Various Substrates. *Advanced Functional Materials* 2020, **30(43)**.
17. Fan C, Xu X, Yang K, Jiang F, Wang S, Zhang Q. Controllable Epitaxial Growth of Core-Shell PbSe@CsPbBr₃ Wire Heterostructures. *Adv Mater* 2018, **30(45)**: e1804707.
18. Zhong Y, Liao K, Du W, Zhu J, Shang Q, Zhou F, *et al.* Large-Scale Thin CsPbBr₃ Single-Crystal Film Grown on Sapphire via Chemical Vapor Deposition: Toward Laser Array Application. *ACS Nano* 2020, **14(11)**: 15605-15615.
19. Geng X, Wang F, Tian H, Feng Q, Zhang H, Liang R, *et al.* Ultrafast Photodetector by Integrating Perovskite Directly on Silicon Wafer. *ACS Nano* 2020, **14(3)**: 2860-2868.

20. Zhao L, Gao Y, Su M, Shang Q, Liu Z, Li Q, *et al.* Vapor-Phase Incommensurate Heteroepitaxy of Oriented Single-Crystal CsPbBr₃ on GaN: Toward Integrated Optoelectronic Applications. *ACS Nano* 2019, **13**(9): 10085-10094.
21. Li Y, Wang X, Wu S, Ci H, Xu H, Li X, *et al.* Large-scale aligned crystalline CH₃NH₃PbI₃ perovskite array films. *Journal of Materials Chemistry A* 2015, **3**(37): 18847-18851.
22. Hill JC, Koza JA, Switzer JA. Electrodeposition of Epitaxial Lead Iodide and Conversion to Textured Methylammonium Lead Iodide Perovskite. *ACS Appl Mater Interfaces* 2015, **7**(47): 26012-26016.
23. Kelso MV, Mahenderkar NK, Chen Q, Tubbesing JZ, Switzer JA. Spin coating epitaxial films. *Science* 2019, **364**(6436): 166-169.
24. Chen Z, Dong Q, Liu Y, Bao C, Fang Y, Lin Y, *et al.* Thin single crystal perovskite solar cells to harvest below-bandgap light absorption. *Nat Commun* 2017, **8**(1): 1890.
25. Gu Z, Huang Z, Li C, Li M, Song Y. A general printing approach for scalable growth of perovskite single-crystal films. *Science Advances* 2018, **4**(6): eaat2390.
26. Lv Q, Lian Z, He W, Sun J-L, Li Q, Yan Q. A universal top-down approach toward thickness-controllable perovskite single-crystalline thin films. *Journal of Materials Chemistry C* 2018, **6**(16): 4464-4470.

27. Chen C, Hu X, Lu W, Chang S, Shi L, Li L, *et al.* Elucidating the phase transitions and temperature-dependent photoluminescence of MAPbBr₃ single crystal. *Journal of Physics D: Applied Physics* 2018, **51**(4).
28. Wang Y, Shi Y, Xin G, Lian J, Shi J. Two-Dimensional van der Waals Epitaxy Kinetics in a Three-Dimensional Perovskite Halide. *Crystal Growth & Design* 2015, **15**(10): 4741-4749.
29. Adesida I, Agarwala S, Caneau C, Bhat R. Highly selective etching of InGaAs on InAlAs in HBr plasma. 1993 (5th) International Conference on Indium Phosphide and Related Materials; 1993 19-22 April 1993; 1993. p. 529-532.
30. Krueger CW, Wang CA, Flytzani - Stephanopoulos M. Vapor etching of GaAs and AlGaAs by CH₃I. *Applied Physics Letters* 1992, **60**(12): 1459-1461.
31. Osherov A, Ezersky V, Golan Y. The role of solution composition in chemical bath deposition of epitaxial thin films of PbS on GaAs(100). *Journal of Crystal Growth* 2007, **308**(2): 334-339.
32. Murza V, Friedman O, Vradman L, Golan Y. Liquid flow deposition of PbS films on GaAs(100). *CrystEngComm* 2018, **20**(26): 3765-3771.
33. Luo P, Zhou S, Liu Z, Xia W, Sun L, Cheng J, *et al.* A novel transformation route from PbS to CH₃NH₃PbI₃ for fabricating curved and large-area perovskite films. *Chem Commun (Camb)* 2016, **52**(75): 11203-11206.

34. Perez M, Peled SaS, Templeman T, Osherov A, Bulovic V, Katz EA, *et al.* A Two-Step, All Solution Process for Conversion of Lead Sulfide to Methylammonium Lead Iodide Perovskite Thin Films. *Thin Solid Films* 2020, **714**.
35. Ning Z, Gong X, Comin R, Walters G, Fan F, Voznyy O, *et al.* Quantum-dot-in-perovskite solids. *Nature* 2015, **523**(7560): 324-328.
36. Rideout VL. An Improved Polishing Technique for GaAs. *Journal of The Electrochemical Society* 1972, **119**(12): 1778.
37. Osherov A, Ezersky V, Golan Y. Hetero-Twinning in Chemical Epitaxy of PbS Thin Films on GaAs Substrates. *Crystal Growth & Design* 2012, **12**(8): 4006-4011.
38. Meng F, Morin SA, Jin S. Growth of Nanomaterials by Screw Dislocation. In: Vajtai R (ed). *Springer Handbook of Nanomaterials*. Springer Berlin Heidelberg: Berlin, Heidelberg, 2013, pp 639-664.
39. Deal BE, Grove AS. General Relationship for the Thermal Oxidation of Silicon. *Journal of Applied Physics* 1965, **36**(12): 3770-3778.

Acknowledgements

This work is supported by the Tsinghua University Initiative Scientific Research Program, the State Key Laboratory of New Ceramic and Fine Processing Tsinghua University (No. KF202108), Beijing Municipal Natural Science Foundation (4202032), National Natural Science Foundation of China (NSFC) (52171239, T2122010).

Author contributions

X. S. and D. K. developed the concepts. D. K., E. W., K. Z., and H. W. performed material growth and characterization. D. K., Y. Z., D. C, and X. S. performed modeling and simulations. K. L., L. Y. and X. S. supervised the research. D. K. and X. S. wrote the paper in consultation with other authors.

Competing interests

The authors declare no competing interests.

Data and materials availability

All data needed to evaluate the conclusions in the paper are present in the paper and/or the Supplementary information.

Figure 1

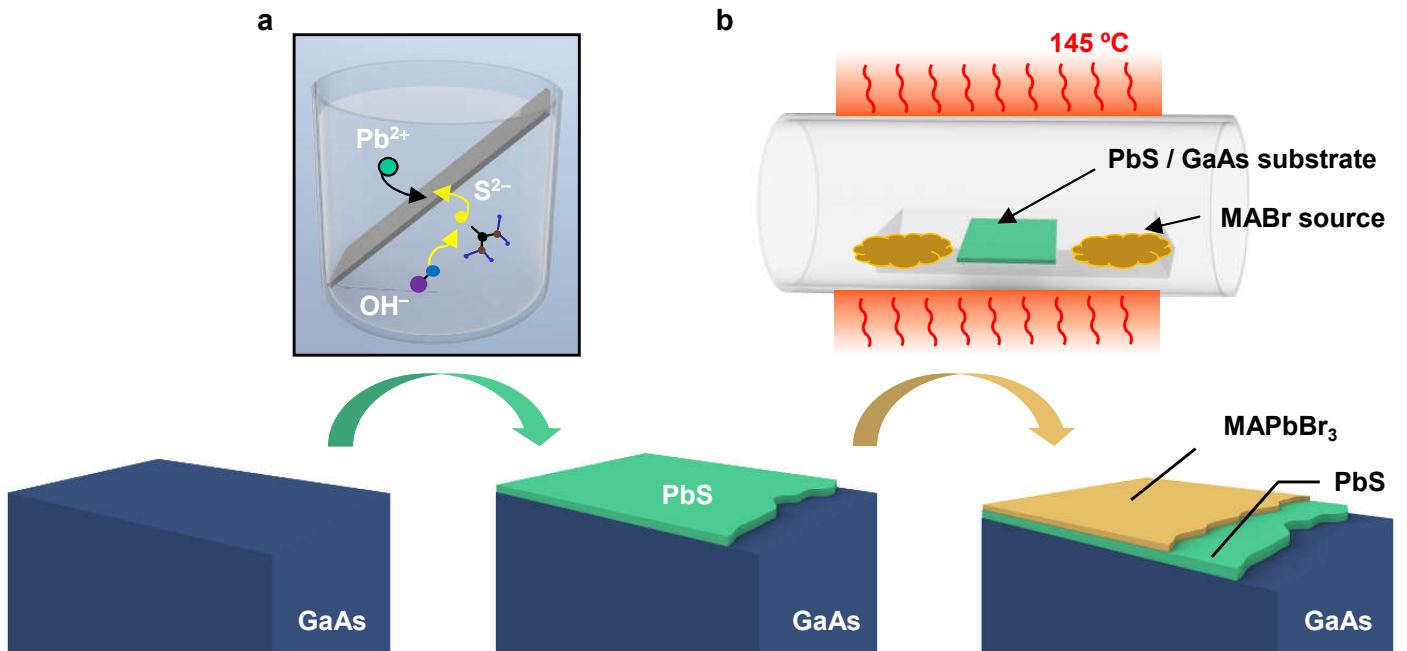


Figure 1. Schematic illustration of the MAPbBr₃ epitaxy on GaAs. (a) A single crystalline PbS film is grown on GaAs via chemical bath deposition. (b) The PbS film then reacts with MABr in a chemical vapor deposition tube to form a single crystalline MAPbBr₃ film.

Figure 2

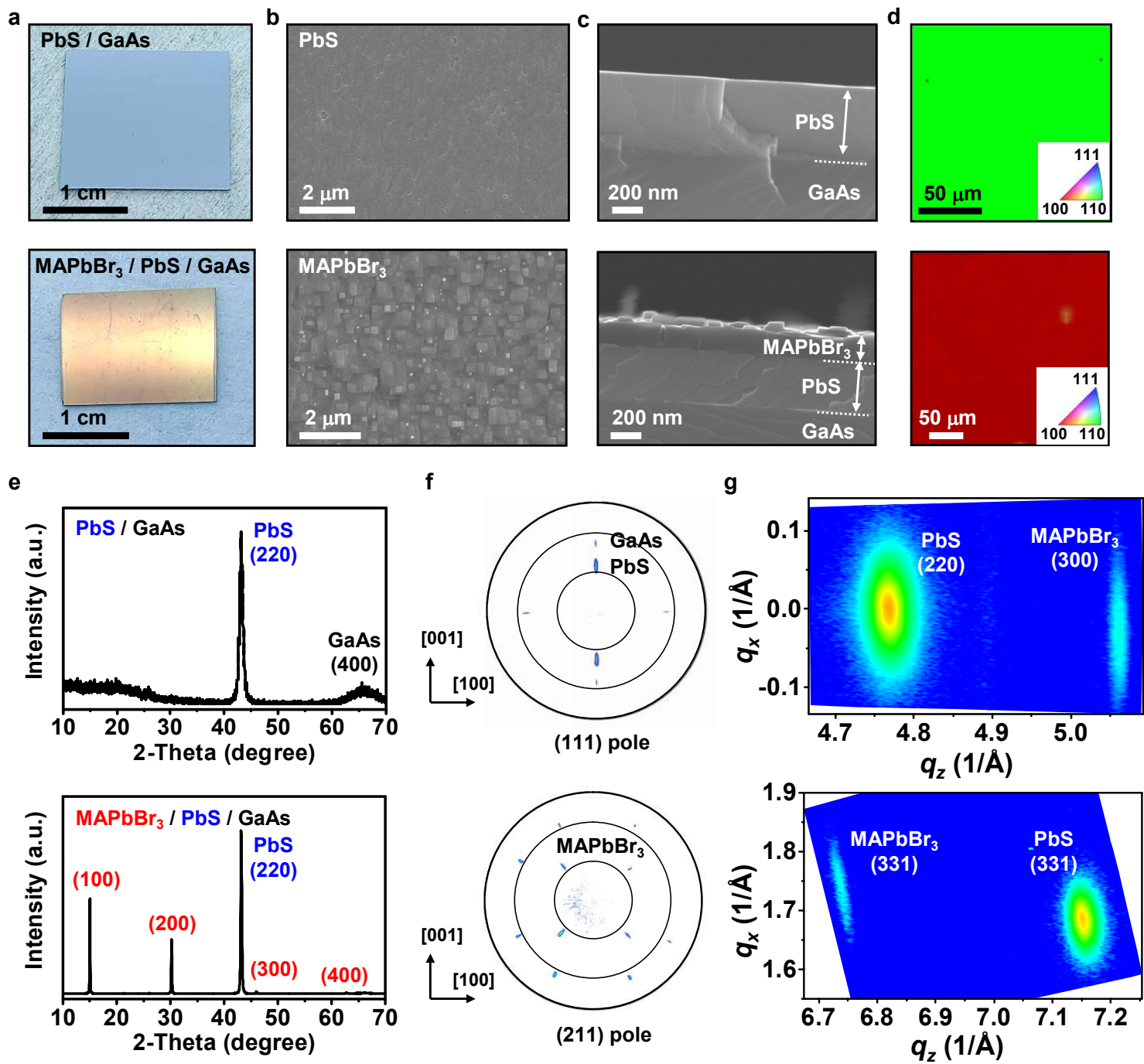


Figure 2. Structural characterizations for PbS-on-GaAs and MAPbBr₃-on-PbS-on-GaAs samples. (a) Top-view photographs, (b) Top-view SEM images, (c) Cross-sectional SEM images, (d) EBSD maps, (e) XRD patterns, and (f) Pole figures for two samples (top: PbS/GaAs; bottom: MAPbBr₃/PbS/GaAs). (g) RSMs around (300) and (331) points of MAPbBr₃.

Figure 3

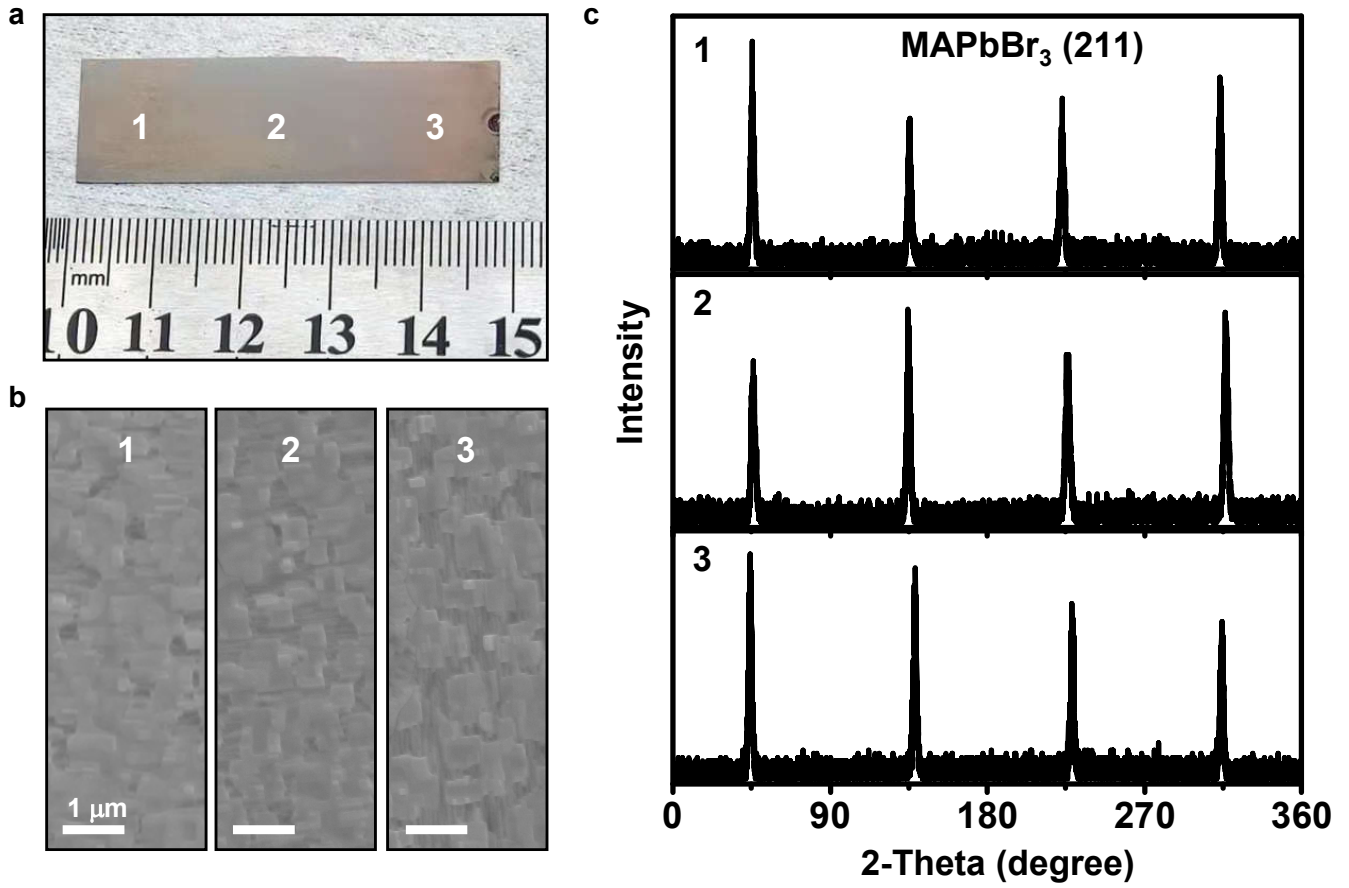


Figure 3. A large-area single crystalline MAPbBr₃ film on PbS/GaAs. (a) Photograph of the sample with a dimension of 1.5 × 5 cm². (b) Top-view SEM images at 3 different locations. (c) XRD phi-scan patterns of the MAPbBr₃ (211) plane at 3 different locations.

Figure 4

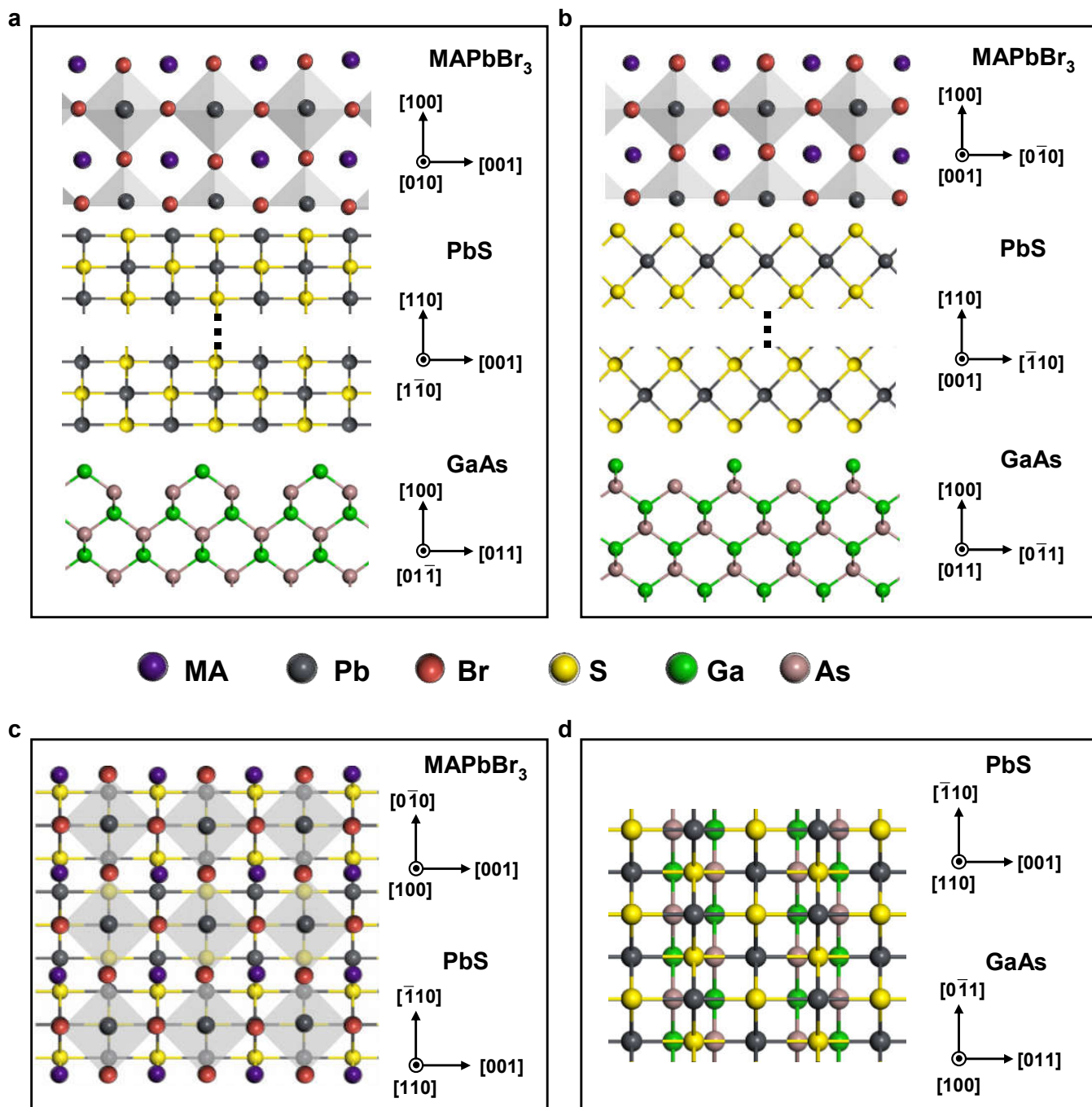


Figure 4. Atomic model of the MAPbBr₃/PbS/GaAs epitaxial structure. (a) Side view normal to the PbS [110] direction. (b) Side view normal to the PbS [001] direction. (c) Top view of the stacked MAPbBr₃ (100) / PbS (220) heterointerface. (d) Top view of the stacked PbS (220) / GaAs (100) heterointerface.

Figure 5

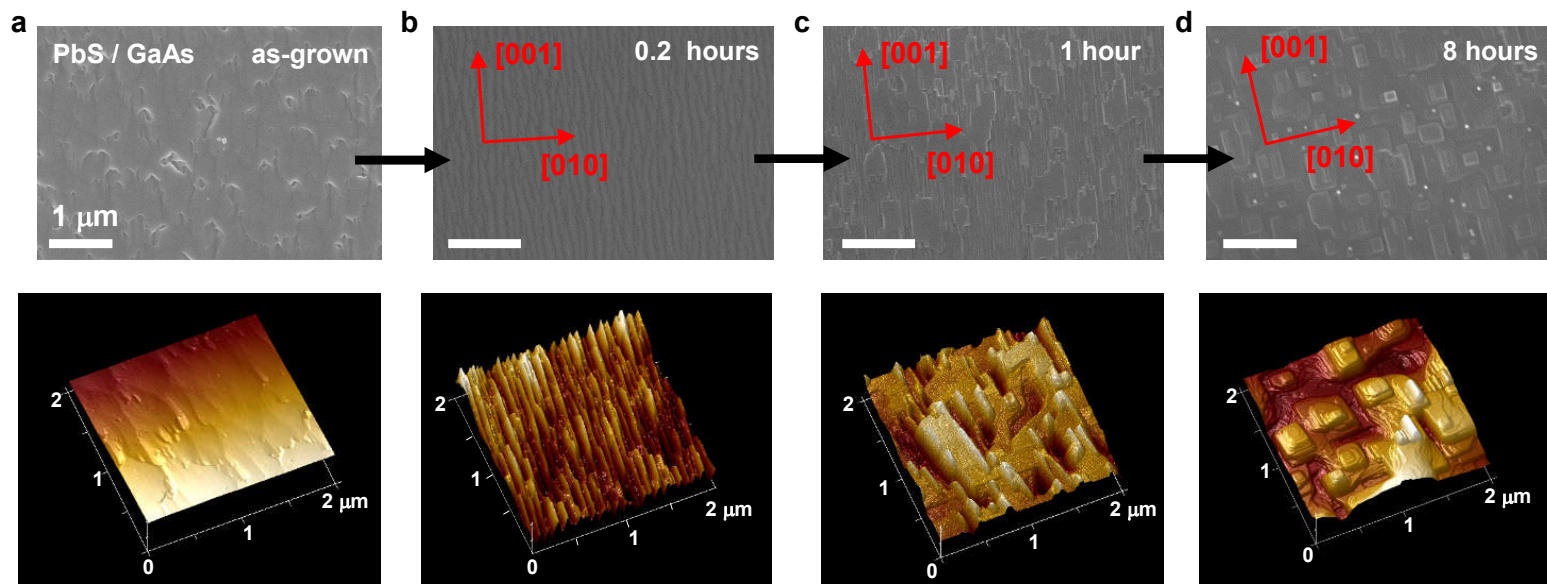


Figure 5. Evolution of surface morphology during the MAPbBr₃ epitaxy on PbS/GaAs. SEM (top) and AFM (bottom) images for (a) the as-grown PbS/GaAs sample, and after growth for (b) 0.2 hours, (c) 1 hour and (d) 8 hours. Arrows indicate the crystal directions of MAPbBr₃.

Figure S1

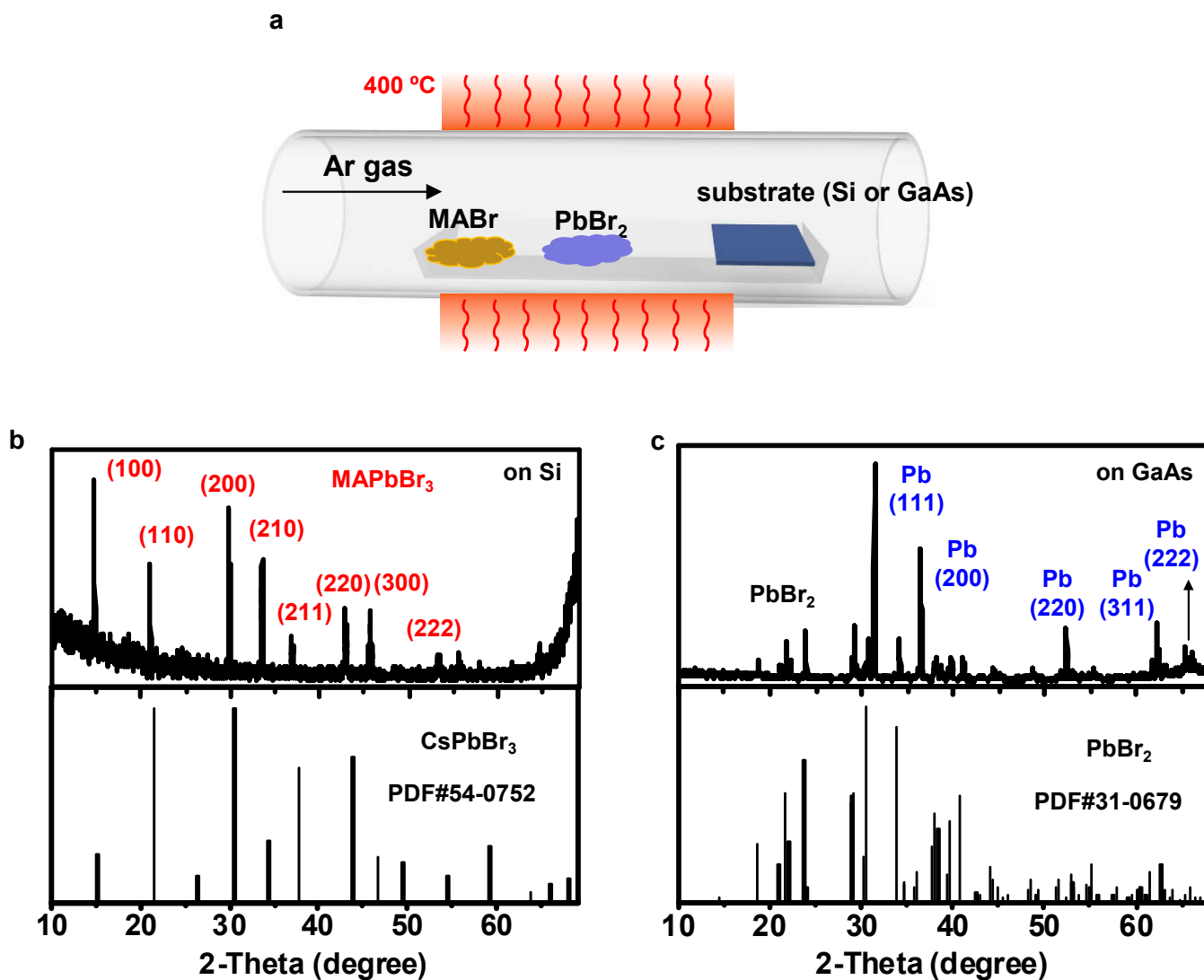


Figure S1. (a) MAPbBr₃ growth via conventional CVD, by reacting MABr and PbBr₂ on Si or GaAs at 400 °C in argon environment. (b) XRD pattern for the CVD deposited film on Si, indicating the formation of polycrystalline MAPbBr₃. (c) XRD pattern for the CVD deposited film on GaAs, indicating the formation of polycrystalline PbBr₂ and Pb, but no MAPbBr₃. Powder Diffraction Files (PDF) of CsPbBr₃ and PbBr₂ are provided for comparison.

Figure S2

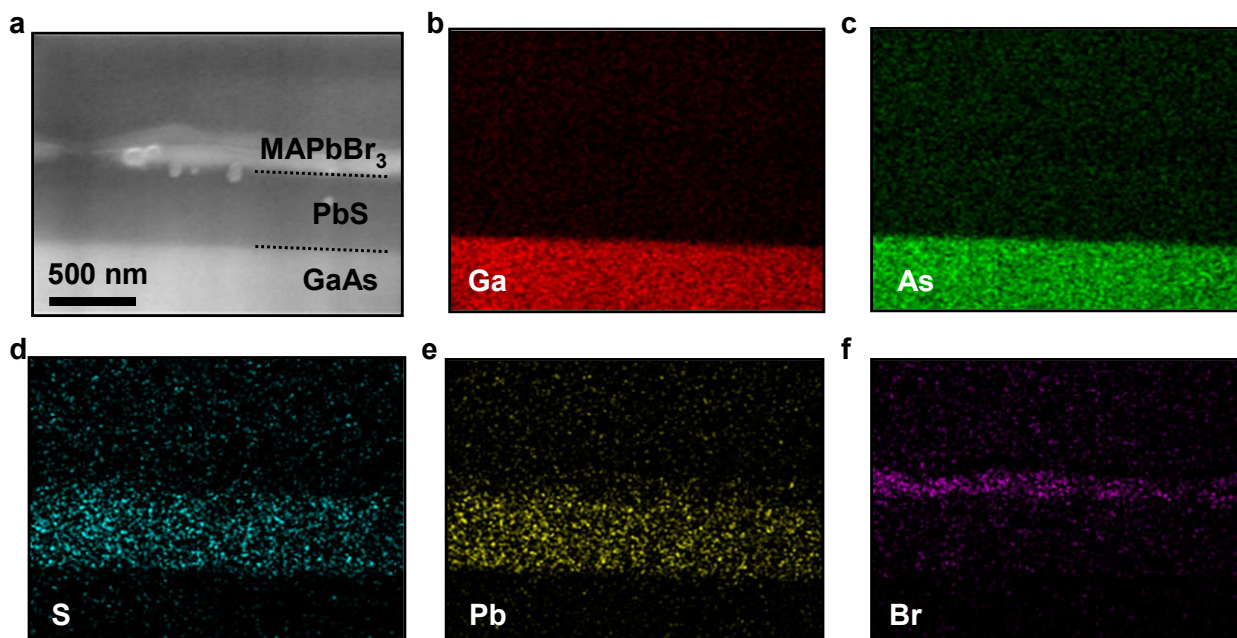


Figure S2. (a) Cross-sectional SEM image and (b–f) corresponding energy-dispersive X-ray spectroscopy (EDS) element mappings for the MAPbBr₃/PbS/GaAs sample.

Figure S3

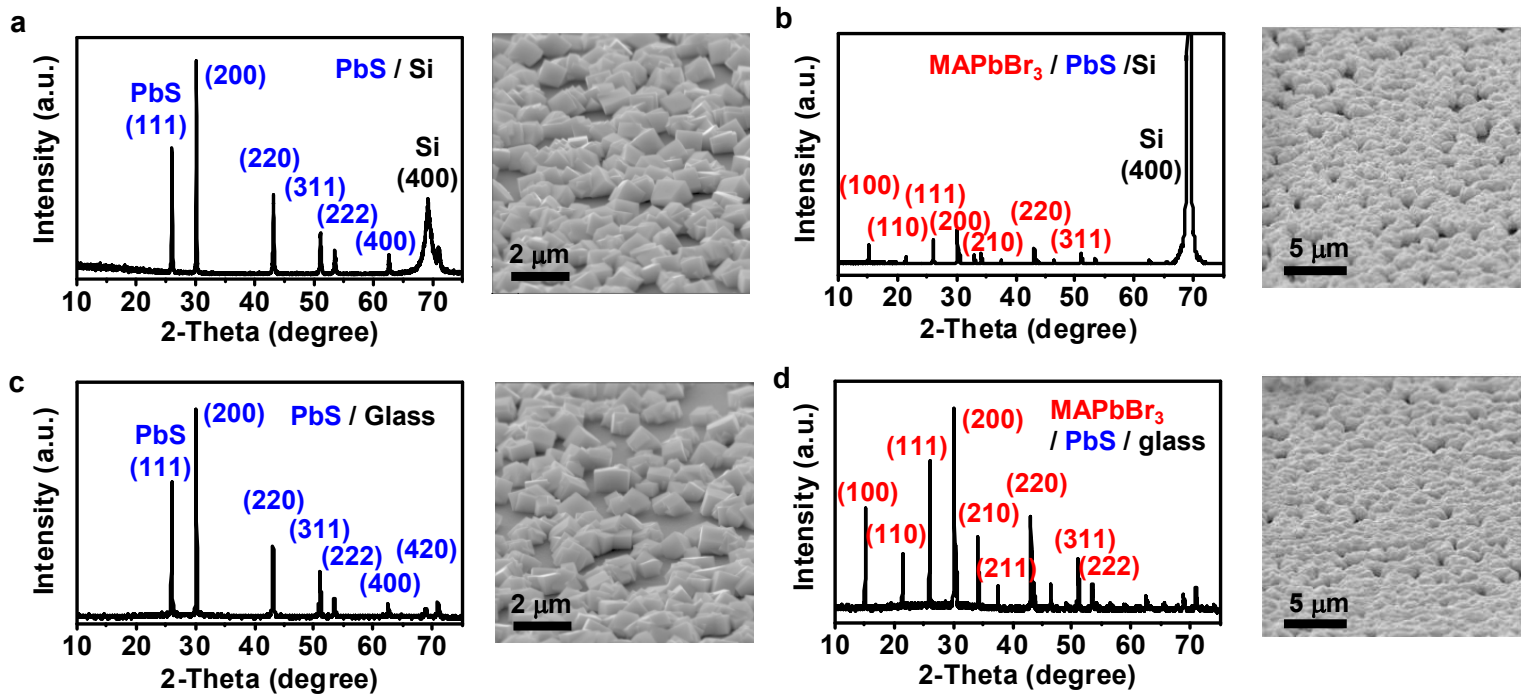


Figure S3. Structural characterizations of PbS and MAPbBr₃ films grown on Si and glass substrates via the same process as in Figure 1. XRD patterns (left) and SEM images (right) for (a) PbS on Si, (b) MAPbBr₃ on PbS/Si, (c) PbS on glass, (d) MAPbBr₃ on PbS/glass. All these films are polycrystalline.